A&A 617, A40 (2018)
https://doi.org/10.1051/0004-6361/201833120

Astronomy & Astrophysics

Spectroscopic EUV observations of impulsive solar energetic particle event sources

R. Bučík[1,2], A. Fludra[3], R. Gómez-Herrero[4], D. E. Innes[2], B. Kellett[3], R. Kumar[5], and Š. Mackovjak[6]

[1] Institut für Astrophysik, Georg-August-Universität Göttingen, 37077 Göttingen, Germany
[2] Max-Planck-Institut für Sonnensystemforschung, 37077 Göttingen, Germany
e-mail: bucik@mps.mpg.de
[3] STFC Rutherford Appleton Laboratory, Didcot OX11 0QX, UK
[4] Space Research Group, University of Alcalá, 28871 Alcalá de Henares, Spain
[5] Department of Astrophysical Sciences, Princeton University, Princeton, NJ 08544, USA
[6] Institute of Experimental Physics, Slovak Academy of Sciences, Watsonova 47, Košice, Slovakia

Received 28 March 2018 / Accepted 1 July 2018

ABSTRACT

Context. Remote observations of solar flare ion acceleration are rather limited. Theoretical predictions for signatures of ion acceleration in extreme ultraviolet (EUV) line profiles have been made. Previous tests involve observations of flares with no evidence for energetic ions.
Aims. We aim to examine a source flare of impulsive (or ^{3}He-rich) solar energetic particle events with EUV line spectroscopy.
Methods. We inspected all (more than 90) reported ^{3}He-rich flares of the previous solar cycle 23 and found only 4 (recurrent) jets in the field of view of the Coronal Diagnostic Spectrometer (CDS) on board the Solar and Heliospheric Observatory (SOHO). The jet with the most suitable spatial and temporal coverage was analyzed in detail.
Results. Two enhanced (nonthermal) line broadenings are observed in the cooler chromospheric and transition-region lines, and they are localized near the site where the closed magnetic loops reconnect with the open magnetic field lines. The enhanced broadenings are both found at the sites with redshifts in the lines, surrounded by the region with blueshifts. One enhanced line broadening is associated with a small flare without energetic particle signatures, while another occurs just after the particle acceleration signatures of the main flare terminated.
Conclusions. The observed excess broadening does not appear to be directly related to the energetic ion production and motions. Further investigations are required that cover the critical impulsive phase of the flare, ideally with high-resolution spectrometers that are specifically pointed to the ^{3}He-rich solar energetic particle source.

Key words. Sun: particle emission – Sun: flares – acceleration of particles – magnetic reconnection – techniques: imaging spectroscopy

1. Introduction

Impulsive (or ^{3}He-rich) solar energetic particle (SEP) events are characterized by a peculiar ion composition that is markedly different from the compositions of the corona or the solar wind (Mason 2007, and references therein). The heavy-ion enhancement in the impulsive SEP events is an increasing function of ion mass. For example, Fe is enhanced by a factor of about 10 compared to its coronal abundance, while the enrichment of ultra-heavy (UH) ions easily exceeds an enhancement factor of 100. This pattern is in contrast to the enhancement of low-mass ^{3}He, which reaches factors of up to 10^4. The anomalous composition is thought to be the signature of a unique acceleration process operating at the flare sites. Models of ion acceleration and fractionation in solar flares have commonly included resonant interaction with plasma waves (Fisk 1978; Winglee 1989; Temerin & Roth 1992; Miller 1998; Zhang 2004; Liu et al. 2006; Kumar et al. 2017), although other non-wave mechanisms (scattering on magnetic islands or direct current electric field) have been suggested (e.g., Drake et al. 2009; Fleishman & Toptygin 2013). Electrons are almost always accelerated to subrelativistic speeds in these events, as demonstrated by direct in situ measurements (Reames et al. 1985; Wang et al. 2012) or by detection of type III radio bursts (Reames & Stone 1986; Nitta et al. 2006).

^{3}He-rich SEP events have been associated with minor (mostly B- and C-class) soft X-ray flares (Reames et al. 1988; Reames & Ng 2004; Nitta et al. 2006, 2015; Bučík et al. 2014, 2016). In addition, an inverse correlation between the soft X-ray peak intensity and ^{3}He (UH) enrichment has been reported (Reames et al. 1988; Reames & Ng 2004). ^{3}He-rich flares have commonly been observed as a jet-like form in extreme ultraviolet (EUV; Nitta et al. 2006, 2015; Chen et al. 2015; Bučík et al. 2018) or white-light coronagraph images (Kahler et al. 2001; Wang et al. 2006). The association with jets has been interpreted as evidence for magnetic reconnection involving field lines open to interplanetary space (Shibata et al. 1992). Remote observations of ion acceleration in solar flares are quite limited. The energetic ions do not show clear flare signatures, as energetic electrons do, through the hard X-ray (HXR) bremsstrahlung or radio emissions. Gamma-ray nuclear lines, produced in a bombardment of energetic (>1−10 MeV nucleon^{-1}) ions with ambient nuclei in the chromosphere, were observed only in major (X- or M-class) flares (e.g., Vilmer et al. 2011). Although the

abundances derived from γ-ray lines show ^{3}He and heavy-ion enrichment (Murphy et al. 1991; Mandzhavidze et al. 1999), the γ-ray lines were generally not observed in ^{3}He-rich SEP events (but see Van Hollebeke et al. 1990; Kartavykh et al. 2007, for the exceptions).

There are theoretical predictions for the formation of asymmetrical broadened profiles (extended red wings) in H I Lyman-α (1216 Å) and He II Lyman-α (304 Å) atomic lines (e.g., Orrall & Zirker 1976; Canfield & Chang 1985; Peter et al. 1990; Brosius & Woodgate 1999) caused by the accelerated ions in solar flares. Specifically, the low-energy (<1 MeV nucleon^{-1}) protons or α-particles (invisible in γ-ray lines) can capture electrons through charge-exchange with thermal neutral hydrogen in the chromosphere and radiate nonthermal Doppler-broadened Lyman-α. The profiles are expected to extend rather far into red wings, ~10 Å for H I and 4–5 Å for He II. Similar processes of charge-exchange between suprathermal (keV) protons and residual neutral hydrogen in the corona have been discussed by Laming et al. (2013). The authors have suggested that the suprathermal ions should manifest themselves through extended wings in resonantly scattered chromospheric H I Lyman-α in the corona. However, so far, no clear evidence of Doppler-broadened Lyman-α from energetic ions in solar flares has been observed (Brosius 2001; Hudson et al. 2012), although the effect has been reported in a flare on the red dwarf star AU Mic (Woodgate et al. 1992). Brosius (2001) has examined a C-class flare with the Coronal Diagnostic Spectrometer (CDS) on board the Solar and Heliospheric Observatory (SOHO) for a signal of enhanced red wings in the profile of He II Lyα line. Hudson et al. (2012) have examined nine hard X-ray/γ-ray events (in M- or X-class flares) for signatures of broad wings in He II Lyα using the full-Sun EVE instrument on board SDO. The authors discuss that strong chromospheric heating during the flare may reduce or mask the charge-exchange mechanism. Jeffrey et al. (2016, 2017) have analyzed the Fe XVI 262.98 Å and Fe XXIII 263.76 Å line profiles observed by the Hinode EIS in two X-class flares and found the profiles consistent with a kappa distribution of emitting ions, with kappa values corresponding to the highly accelerated ion distribution. The authors have speculated that flare-accelerated Fe ions could account for the observed excess broadening.

A suitable candidate for EUV spectral line investigations, with a low background, may be ^{3}He-rich SEP events, whose solar sources have been associated with minor X-ray flares or weak EUV brightenings. In addition, in such events, we have direct evidence for ion acceleration in the flare via in situ measurements of energetic ion fluxes. In this study, we present the first observations of EUV spectral lines in the source flare of ^{3}He-rich SEPs.

2. Methods

We study the solar source of ^{3}He-rich SEPs with the CDS (Harrison et al. 1995) on board the SOHO. The CDS consists of normal incidence (NIS) and grazing incidence (GIS) spectrometers. The observations examined in this study were obtained with NIS using a $4'' \times 240''$ slit to produce a raster image. The NIS covers the 307–379 Å and 513–633 Å wavelength ranges, with approximate spectral resolutions of 0.32 Å and 0.54 Å at full width at half-maximum (FWHM), respectively. The following three lines are examined: He I 584.30 Å, O V 629.39 Å, and Fe XVI 360.80 Å, corresponding to the formation temperatures ~0.03 MK, 0.25 MK, and 2.5 MK, respectively. These CDS lines have been analyzed in several previous studies on solar flares (e.g., Czaykowska et al. 1999; Milligan et al. 2006a,b; Teriaca et al. 2006). We recall that He I stands for neutral helium, O V is 4 times ionized oxygen with a charge-to-mass ratio $Q/A = 4/16$, and Fe XVI is 15 times ionized iron with $Q/A = 15/56$. We also examined EUV images of the ^{3}He-rich solar source obtained by SOHO Extreme-ultraviolet Imaging Telescope (EIT; Delaboudinière et al. 1995) and the Transition Region and Coronal Explorer (TRACE; Handy et al. 1999), and magnetograms obtained by the SOHO Michelson Doppler Imager (MDI; Scherrer et al. 1995). The ^{3}He-rich SEPs were analyzed using the measurements from the SOHO Electron Proton Helium Instrument (EPHIN; Müller-Mellin et al. 1995). The EPHIN, a $\mathrm{d}E/\mathrm{d}x$ versus E telescope, measures hydrogen and helium isotopes in the range 4 MeV nucleon^{-1} to >53 MeV nucleon^{-1}. We also inspected dynamic radio spectra for the event-associated type III radio bursts. The radio data are provided by the Wind WAVES instrument (Bougeret et al. 1995) at a frequency range (<14 MHz), which covers emission generated from about $2\,R_\odot$ to 1 au and the Phoenix-2 (Bleien, Switzerland) broadband spectrometer (Messmer et al. 1999), which is operated in the frequency range 0.1–4 GHz. Furthermore, we made use of soft and HXR observations made with the NOAA GOES-10 X-ray and Wind KONUS (Aptekar et al. 1995) sensors, respectively. The interplanetary magnetic field (IMF) and solar wind speed measurements were provided by the Magnetic Field Experiment (MAG; Smith et al. 1998) and Solar Wind Electron Proton Alpha Monitor (SWEPAM; McComas et al. 1998) instruments on board ACE. While SOHO, ACE, and Wind were in interplanetary space, the TRACE spacecraft was in geocentric orbit.

To find a ^{3}He-rich solar source in the CDS field of view (FOV), we inspected all (93) ^{3}He-rich SEP events of the previous solar cycle 23 that had a reported solar source (Mason et al. 2002; Nitta et al. 2006; Wang et al. 2006). The solar sources in 67 events have been identified by Nitta et al. (2006), in another 19 events, they were reported by Wang et al. (2006), and in 7 events, by Mason et al. (2002). These events are from the period September 1997 to March 2003. The CDS started scientific operation in April 1996. To identify the solar source of a ^{3}He-rich SEP event, Wang et al. (2006) examined Hα and SOHO EIT flares within a few hours of the estimated ion injection time, Nitta et al. (2006) examined type III radio bursts in the five-hour window preceding the observed ion onset and then searched for the associated brightening in SOHO EIT coronal images, and Mason et al. (2002) selected the event-associated X-ray flare based on the estimated ion injection time. Overlays of the CDS FOV with other imaging instruments on board SOHO are subject to a 5″ pointing uncertainty of the CDS (Fludra 2001).

We found only four ^{3}He-rich SEP source flares that were fully or partially covered by the CDS FOV. All these flares were from the same active region, which has the NOAA number 10069. Figure 1 shows SOHO EIT or TRACE EUV images of these ^{3}He-rich SEP sources and superimposed CDS FOVs. Figures 1a,c indicate that the flares in events 1 and 3 were only partially captured with the CDS. The flare in event 2 was quite well captured (see Fig. 1b) and therefore is further investigated in detail. In event 4 only the post-flare phase was captured (see Fig. 1d). A dimming jet exhibits an interesting twisted configuration in event 4. Table 1 shows some characteristics of these flares and the associated particle events. Column 1 lists the event number, Col. 2 the particle event start time, and Col. 3 the type III radio burst start time. Columns 4, 5, 6, and 7 indicate the GOES X-ray flare start time, time at the flare maximum, the flare location, and class, respectively. Columns 8 and 9 provide

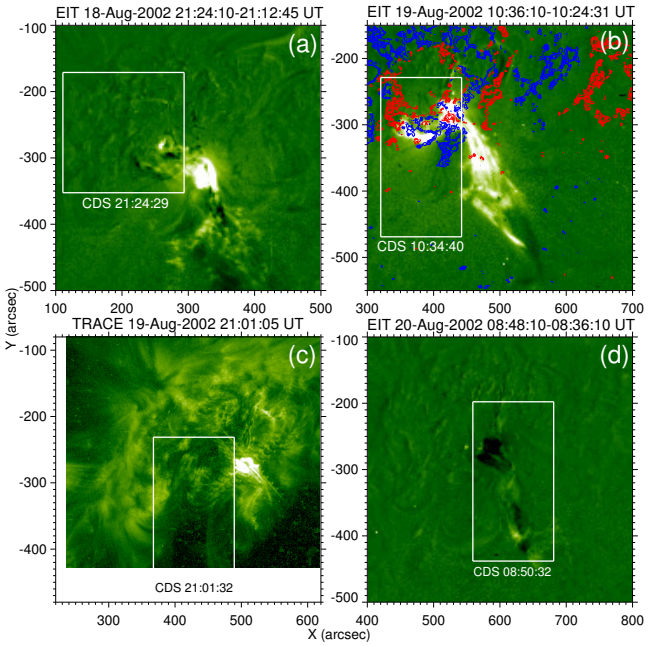

Fig. 1. SOHO EIT 195 Å EUV 12 min running-differences images for flares in event 1 (*panel a*), event 2 (*panel b*), and event 4 (*panel d*). Overplotted in *panel b* are ±500 G SOHO MDI magnetogram data contours for 2002 August 19 11:11 UT, where blue and red show positive and negative polarity. TRACE 195 Å EUV direct image (rescaled to L1 and aligned with the CDS Fe XVI 360.80 Å line raster image) for event 3, for which SOHO EIT data are not available (*panel c*). The empty area at the bottom of (*panel c*) is due to the restricted TRACE FOV. White rectangles depict the CDS FOV. While the images in events 1, 2, and 3 are near (±1−2 min) the flare maximum, the image in event 4 is taken ~20 min after the flare maximum.

the ^{3}He/^{4}He and Fe/O abundance ratios, respectively. Table 2 lists some parameters of CDS studies that match these ^{3}He-rich flares. Column 1 gives the event number, Col. 2 the start time of the raster image, Col. 3 the duration of the rastering, Col. 4 the temporal resolution, and Col. 5 the exposure time. Columns 6, 7, and 8 indicate the CDS pointing, FOV, and the spatial resolution, respectively. Columns 9 and 10 indicate the names of the CDS studies and their total durations, respectively. The observational mode in event 2 includes the four lines He I, O V, Mg IX, and Fe XVI.

3. Results

Events 1–4 have been included in previous studies (see references in Table 1). All these events were associated with M-class flares. The events exhibited high ion intensities at high energies (>10 MeV nucleon^{-1}) and are therefore called large impulsive SEP events (Reames & Ng 2004), as opposed to more typical small impulsive events. The events are electron-rich (or proton-poor), as reported in a study of Cane et al. (2010). The events showed large enhancements of trans-Fe elements by a factor of 10^2–10^3 for $Z > 50$ (Reames & Ng 2004). The measured abundances in events 2–4 are consistent with a coronal temperature 2.5–3 MK in their source (Reames et al. 2014). Wiedenbeck et al. (2010) have performed a detailed elemental and isotopic compositional analysis of the measurements above 10 MeV nucleon^{-1} in event 4 (2002 August 20). Based on the inferred charge states (assuming Q/A-dependent fractionation), the best-fit temperature in the source plasma was found to be ~4 MK, with large deviations to higher temperatures for Fe–Ni. The authors also reported a temperature of ~1.6 MK, assuming a possible Q^2/A law. They also reported observed Fe charge states Q between 18 (Fe XIX) and 22 (Fe XXIII) at low energies (0.25–1 MeV nucleon^{-1}). The 2002 August 20 event was the largest impulsive event in solar cycle 23 observed at energies >10 MeV nucleon^{-1} (Leske et al. 2003).

The EUV flare type in the investigated event 2 has been noted as an ejection in 195 Å SOHO EIT images in Wang et al. (2006). Examining the TRACE 195 Å images, the flare type in all four events 1–4 has been noted as a jet in Nitta et al. (2006). The SOHO EIT flare in event 2 occurred close to a new emergence of a negative-polarity flux observed with SOHO MDI magnetograms between 2002 August 19 01:36–11:25 UT (Tan & Yan 2008). Using the Nançay Radio-Heliograph observations at 164 MHz, Tan & Yan (2008) found that the metric type III radio bursts were located near the top of the loops at height ~0.15 $R_\odot$. Events 3 and 4 have been included in a study on electron acceleration in solar jets (Krucker et al. 2011). A HXR imaging with RHESSI showed three chromospheric (HXR) sources in event 4, two at the loop footpoints, and one related to the open field line. In event 3 only two chromospheric sources were seen, where a third source could be hidden by the extended flare (Krucker et al. 2011). The authors found the onset of the EUV jets observed with TRACE coincident with the HXR emission. For event 2 no RHESSI solar data are available for the associated flare at ~10:07−10:41 UT on 2002 August 19.

The potential-field source-surface (PFSS) extrapolations of the photospheric magnetic field (National Solar Observatory synoptic maps) in event 2 show the Earth-directed open field lines near the associated flare (Wang et al. 2006). Specifically, the field lines that cross the source surface at longitudes between W35 and W65 and at latitudes lower than 20° from the ecliptic (but not those directed to the ecliptic) were rooted next (<4°) to the event source. Wang et al. (2006) have noted that a dipole field line that intersects the source surface at 20° would continue to bend equator-ward beyond the source surface. The PFSS extrapolations based on the MDI magnetograms assimilated into the evolving surface flux model show no open field lines within 10° from the flare location (Nitta et al. 2006). Using the Wilcox Solar Observatory synoptic maps, the authors report open field lines with a combined offset at the photosphere (from the associated flare) and at the source surface (from the Parker spiral footpoint) of less than 10°. It has been pointed out that the PFSS extrapolated field depends to some extent on the input magnetograms (Nitta et al. 2006).

3.1. ^{3}He-rich SEP events 1–4

Owing to the limited element resolution of the Wind LEMT instrument, only an upper limit of 0.2 has been obtained for the ^{3}He/^{4}He ratio in events 1–4 at 2.1–2.5 MeV nucleon^{-1} (Reames & Ng 2004). Figure 2 shows SOHO EPHIN measurements of ^{3}He-rich SEP events 1–4 in the period 2002 August 18 (day 230) 12:00 UT–August 21 (day 233) 00:00 UT. The ions with a parallel incidence are selected, which improves the isotopic resolution at the cost of decreased statistics. Therefore, ^{3}He shows only a small increase near the detection limit in event 1. The upper panel of Fig. 2 shows the 0.7–3.0 MeV electron intensity, and the 10–25 MeV nucleon^{-1} ^{3}He and ^{4}He intensities; the lower panel shows the helium mass spectrogram. All four ^{3}He-rich SEP events were accompanied by relativistic electron events. Event 2 shows the highest ^{3}He intensity and a large ^{3}He enrichment. A possible ion event associated with the

Table 1. ^{3}He-rich SEP event properties.

Event	SEP start[a]	Type III start[b]	1–8 Å GOES X-ray flare[c]				^{3}He/^{4}He[d]	Fe/O[e]	Ref.
			Start	Max	Location	Class			
1	2002-Aug-18 23:00	21:10	21:12	21:25	S13W20	M2.2	0.02 ± 0.01	0.40 ± 0.04	1,2,3
2	2002-Aug-19 11:00	10:30	10:28	10:34	S12W26	M2.1	0.42 ± 0.04	1.34 ± 0.04	1,2,3,4,5,6,7
3	2002-Aug-19 23:00	20:57	20:56	21:02	S11W32	M3.1	0.43 ± 0.08	2.12 ± 0.07	1,2,7,8
4	2002-Aug-20 10:00	08:25	08:22	08:26	S11W38	M3.4	0.06 ± 0.02	1.96 ± 0.04	1,2,3,4,7,8,9

Notes. [(a)] Wind LEMT 2–3 MeV nucleon^{-1} (Nitta et al. 2006). [(b)] Wind WAVES 4 kHz–13.8 MHz (Nitta et al. 2006). [(c)] From Nitta et al. (2006) but start time (Start) and time at flux maximum (Max) from the Solar and Geophysical Event Reports compiled by the NOAA Space Weather Prediction Center (SWPC); ftp://ftp.swpc.noaa.gov/pub/warehouse/2002/. [(d)] SOHO EPHIN 5–25 MeV nucleon^{-1} (this work). [(e)] Wind LEMT 3.3–10 MeV nucleon^{-1} (Reames & Ng 2004).
References. (1) Nitta et al. (2006); (2) Reames & Ng (2004); (3) Cane et al. (2010); (4) Leske et al. (2003); (5) Wang et al. (2006); (6) Tan & Yan (2008); (7) Reames et al. (2014); (8) Krucker et al. (2011); (9) Wiedenbeck et al. (2010).

Table 2. SOHO CDS data for ^{3}He-rich SEP sources.

SEP event	Raster start time	Dur. (s)	Tem. res. (s)	Exp. time (s)	Pointing (arcsec)	FOV (arcsec)	Spatial res. (arcsec)	CDS study[a]	
								Name	Dur.
1	2002-Aug-18 21:24:29	681	15.1	8	202.26, −261.81	182.80 × 181.40	4.06 × 3.36	FLARE_AR	8.4
2	2002-Aug-19 10:34:40	318	10.6	5	381.22, −348.87	121.90 × 240.20	4.06 × 1.68	CD5	4.8
3	2002-Aug-19 21:01:32	321	10.7	5	428.32, −351.31	121.90 × 240.20	4.06 × 1.68	CD5	10.1
4	2002-Aug-20 08:50:32	318	10.6	5	620.10, −317.88	121.90 × 240.20	4.06 × 1.68	CD5	2.2

Notes. [(a)] FLARE_AR: Flaring Active Region Study, CD5: Coronal Dynamics; Dur. (h).

second electron increase in event 3 is not included in ^{3}He/^{4}He in Table 1.

The electron onset time in event 2 at the energy range 0.25–0.7 MeV is measured at 10:45 UT ±1 min. Assuming a scatter-free transport along the nominal Parker spiral (length 1.1 au for a measured solar wind speed of ∼500 km s^{-1}), the propagation time for electrons with a mean energy 0.42 MeV (speed 0.84c) would be 11 min. This implies a solar release time at about 10:34 UT. Subtracting a photon travel time of 8.3 min, the type III radio bursts start time at the Sun is at ∼10:22 UT in event 2 (see Table 1). Thus, the inferred release of relativistic electrons is delayed by 12 min from the type III bursts. A longer travel distance and/or scattering during transport may be responsible for the delay (e.g., Kahler et al. 2007). Because of several assumptions, the type III radio burst observations provide a more reliable measurement of the electron release time than the estimate based on electron propagation time. There is no significant proton increase associated with event 2, instead, the event is clear at the helium channels. An accurate timing for ions is difficult because of low statistics, and it is further complicated by the high particle flux, which increases background and causes a decrease of the geometric factor of the instrument at 11:14 UT on August 19. Using the pulse-height analyzed (PHA) data and selecting ^{3}He in a narrow band between 10 and 15 MeV nucleon^{-1}, the estimated onset time is 11:35 ± 10 min. Assuming a mean energy of about 12.2 MeV nucleon^{-1} implies a solar release time at 10:38 ± 10 min, which would be compatible with the electron release time at 10:34 UT.

3.2. Imaging observations of the source in event 2

Figure 3 shows the 122″ × 240″ CDS raster images in O v 629.39 Å line taken during different phases of the ^{3}He-rich flare in event 2. The rasters were built up by scanning the 4″ × 240″ slit from solar west to east over 30 pointing positions in 5 min and ∼19 s. The rasters in the upper panels display the average intensity in the line profile, the panels in the middle row show the line shift relative to the median wavelength obtained from the whole raster, and the bottom panels present the line FWHM. After the temporary loss of SOHO in 1998, the CDS spectral line profiles were found to have changed. To obtain the line shift and width from post-recovery data, we performed a single broadened Gaussian least-squares fit to the line intensity profile in every pixel of the raster. W. T. Thompson (1999)[1] reports a broadened Gaussian function that matches the post-recovery line profiles well. The broadened Gaussian function has two extra parameters to fit the asymmetry wings of the CDS instrumental response. The CDS intensity maps in the upper row of Fig. 3 indicate two distinct brightenings, one at 10:34:40 UT and another at 10:45:37 UT. These intensity brightenings contain small areas of the enhanced line broadenings, as seen in the bottom row of Fig. 3. The panels in the middle row of Fig. 3 indicate that both intensity brightenings roughly correspond to the blueshift (or plasma upflow) region, although the enhanced line broadenings contain redshift (downflow) areas or areas with a reduced upflow velocity (dark blue pixels). The strongest blueshift is seen at 10:51:00 UT, just after the second brightening, and it is not related to the event-associated flare (see Fig. 7a).

Figure 4 depicts the broadened Gaussian fits to the O v line intensity profiles for one of those pixels showing the strong line broadening at 10:34:40 UT and 10:45:37 UT. The quiet line profiles outside the flaring region are also shown. These have widths comparable to the instrumental width. Figure 5 shows the CDS raster images for He I 584.30 Å and Fe XVI 360.80 Å lines at times when the strong O v line broadenings are seen.

[1] See CDS Software Note No. 53 (http://solar.bnsc.rl.ac.uk/swnotes/cds_swnote_53.pdf).

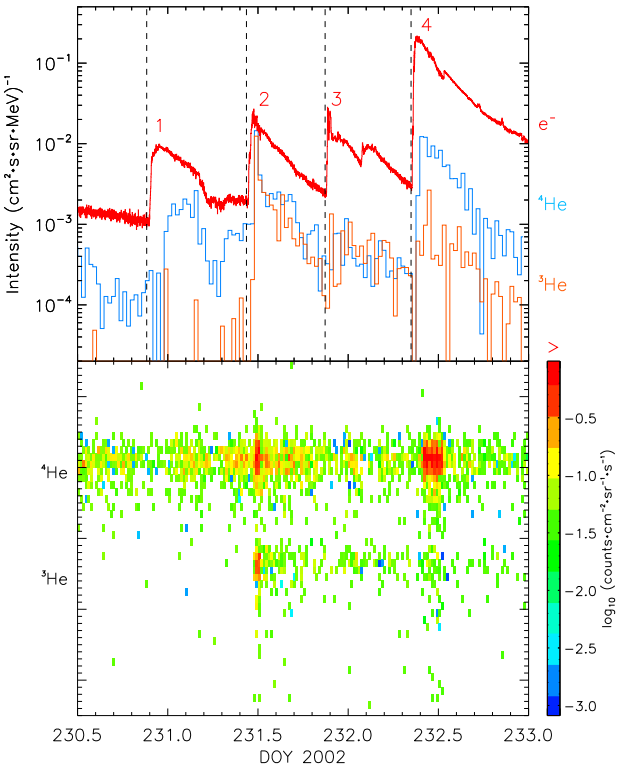

Fig. 2. SOHO EPHIN measurements. *Top*: 1 min averaged 0.7–3.0 MeV electron intensity (divided by 500) and 30 min averaged 10–25 MeV nucleon^{-1} ^{3}He, ^{4}He intensities. Dashed vertical lines indicate X-ray flares associated with events 1–4 (see Table 1). *Bottom*: helium mass spectrogram of individual PHA ions with no energy restriction.

Similarly to O v, the He i line is fit with a single broadened Gaussian function. Since there is a second weaker line on the blue side of the Fe xvi peak (a blend of Fe xiii lines at 359.6 Å and 359.8 Å), the Fe xvi line is fit with a double Gaussian where the FWHM is taken from the stronger central line. The corresponding line broadenings are seen in cooler He i line, but not in the hot Fe xvi line. The He i line broadenings at 10:34:40 and 10:45:37 UT are observed in the regions with the plasma downflows. This is consistent with the observations in the O v line, although the plasma flows are more mixed in the O v line.

The intensity brightening at 10:34:40 UT occupies two separate areas. As indicated in the EIT image (5″ spatial resolution) in Fig. 1b, the brighter area in the west corresponds to the jet locus, and the dimmer region in the east to the top of the closed loop. The locus of the jet originated at the southwest boundary of a large sunspot at the interface with the minor polarity field. The negative IMF polarity during event 2 is consistent with the sunspot polarity field. To show more details of the jet, we plot in Fig. 6 the high-resolution (1″) TRACE 195 Å EUV images at times of the enhanced line broadenings. The pixels with the line broadening at 10:34:40 UT coincide with the jet locus and the area where the coronal closed structure reconnects with the open field lines. During the second line broadening at 10:45:37 UT, a flare/small jet was observed shortly between 10:45–10:50 UT with the TRACE high-cadence (17 s) EUV images. The post-flare arcade of the closed loops is clearly visible in the upper right part of the image in Fig. 6b.

To align between TRACE and SOHO CDS, we first checked the inclinations of different flaring structures in SOHO EIT 195 Å image on 2002 August 19 10:36:10 UT (Fig. 1b) and TRACE 195 Å image on 2002 August 19 10:34:54 UT (Fig. 6a). The time offset of 75 s between these two images corresponds to a negligible 0.1″ in the solar rotation. The alignment was made after rescaling TRACE to L1. It is obvious that no significant rotation is needed to coalign the jet seen in both images. In a further step, the TRACE 195 Å images in Fig. 6 were manually shifted in solar X by +10″ to coalign them with features observed in the CDS Fe xvi 360.80 Å line raster image (Fig. 5). A similar approach was applied to the TRACE image in Fig. 1c. The EIT 195 Å channel includes emission from the bright Fe xii line formed at ~1.6 MK, and therefore the comparison with CDS 2.5 MK Fe xvi line is reasonable.

3.3. X-ray and radio observations in event 2

Figures 7a,b show GOES X-ray flux (1.0–8.0 Å, 0.5–4.0 Å) light curves and a Wind WAVES radio spectrogram during the M2.1 class flare in event 2. A strong type III radio burst was observed during the impulsive (or rapid X-ray flux increasing) phase of the flare. The line broadening observed at the raster 10:34:40 UT (marked by the leftmost solid vertical line) corresponds to the time just after the flare maximum and coincides with the termination of the type III radio burst (or a termination of energetic electron injection into interplanetary space). More accurately, the pixels with the enhanced line broadening were scanned even slightly later at ~10:35:10–10:35:40 UT. The same area was scanned in the previous rastering, at about the flare (and type III burst) onset time at ~10:29:45–10:30:15 UT, but no enhanced line broadening is visible as yet. The excess line broadening at the raster 10:45:37 UT (marked by another vertical solid line) most likely corresponds to another X-ray flare that is not well resolved from the high background during the decay phase of M2.1 flare. The GOES X-ray flux in the M2.1 flare does not continue to decrease to the background values, but forms a plateau at around 10:45 UT that may correspond to the <C2.5 class flare. No type III radio bursts were associated with this second line broadening. Either the jet might have formed along the closed magnetic field lines, and/or the energy release was too weak for a particle acceleration.

After examining full-disk EIT difference images (12 min cadence), we note that the follow-up C3.2 X-ray flare with a maximum at ~10:52 UT on 2002 August 19 (see Fig. 7a) originated in the same active region. Again, no type III radio bursts accompanied this flare. Low-energy electrons (<30 keV), attributed to the source of type III radio bursts (Krucker et al. 1999), have been measured in event 2 with the Wind 3D Plasma and energetic particle instrument (3DP; Lin et al. 1995) in eight energy bins between 1.8 and 19 keV. However, the high pre-event background prevented measuring the onset of the low-energy electron event well.

Figures 7c,d show high-resolution HXR and radio data in a 9-min period, marked by a shaded bar in Figs. 7a,b, covering the impulsive and early decay phase of the M2.1 flare in event 2. The HXR intensity was detected by the Wind KONUS X-ray instrument in two energy channels ~20–80 and ~80–300 keV. Multiple HXR bursts were detected between 10:30:40 and 10:34:00 UT on August 19 (see also the Wind KONUS Solar Flare database[2]). The radio spectra, in the frequency range 0.1–1.0 GHz, were observed with the Phoenix-2 Radio Telescope. A large group of intense type III bursts at 10:30:06–10:33:54 UT

[2] http://www.ioffe.ru/LEA/kwsun/

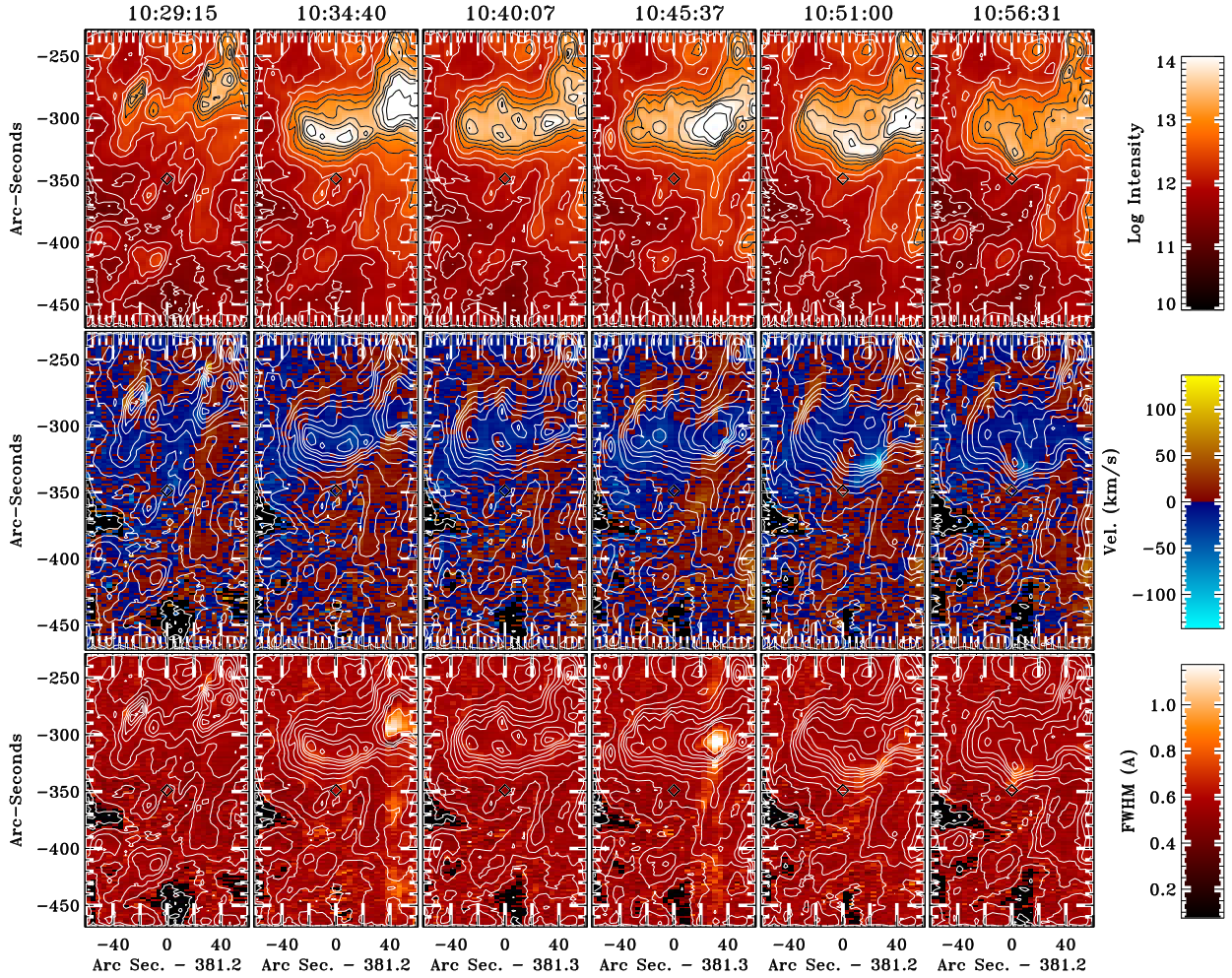

Fig. 3. CDS rasters (O v 629.39 Å line) of the source flare in event 2 between 10:29:15 and 10:56:31 UT on 2002 August 19. Times are given for the beginning of the rastering. *Top row*: intensity (photons s^{-1} cm^{-2} sr^{-1}). *Middle row*: wavelength shift relative to the median wavelength taken from the full image. *Bottom row*: FWHM of the line. The contours for every 0.25 of $\log_{10}$ intensity are overplotted.

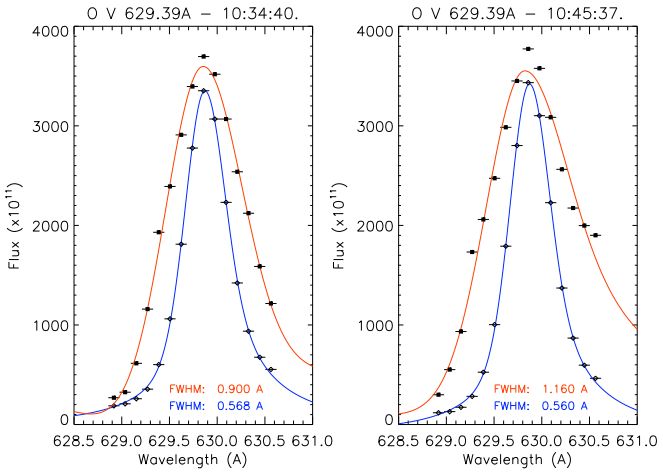

Fig. 4. *Left*: broadened Gaussian fits to the O v intensity (photons s^{-1} cm^{-2} sr^{-1}) from the pixel (420″, −290″; red curve) and to the intensity summed over 90 pixels (to obtain a similar level of counts) around (370″, −420″; blue curve) at 10:34:40 UT on August 19. *Right*: similar to the left panel, but at 10:45:37 UT on August 19, and the red curve shows the pixel (410″, −310″).

coincides with HXR bursts, indicating that their parent energetic electrons are related to the same acceleration episodes. The NOAA NGDC Solar Radio Bursts Report[3] lists a large group of decimetric (DCIM) bursts (>10) at 10:30:18–10:34:06 UT in the frequency range 2.0–4.5 GHz (Ondřejov). Just above the range of the WAVES instrument, the type III bursts continue in the range 20–100 MHz observed with the Artemis-IV (Thermopylae) radiospectrograph.

4. Discussion and further prospects

Spectral line broadening is usually caused by thermal ion motion. In solar flares the excess (non-thermal) line broadening has been often observed (e.g., Fludra et al. 1989). It has been discussed that the excess broadening observed in EUV spectral lines may be an indicator of unresolved plasma flows (e.g., Milligan 2011), wave turbulence (e.g., Moortel & Nakariakov 2012), or accelerated nonthermal ion motions (e.g., Jeffrey et al. 2016).

Jeffrey et al. (2017) have reported that a velocity distribution emitting from the Fe XVI ($Q/A = 15/56$) line has a higher excess broadening than the Fe XXIII ($Q/A = 22/56$) velocity distribution. This would be consistent with the measured heavy-ion enhancement that increases with low Q/A ratio in ^{3}He-rich flares (Reames & Ng 2004; Mason et al. 2004) as well as with

[3] ftp://ftp.ngdc.noaa.gov/STP/space-weather/solar-data/solar-features/solar-radio/radio-bursts/reports/spectral-listings/2002/

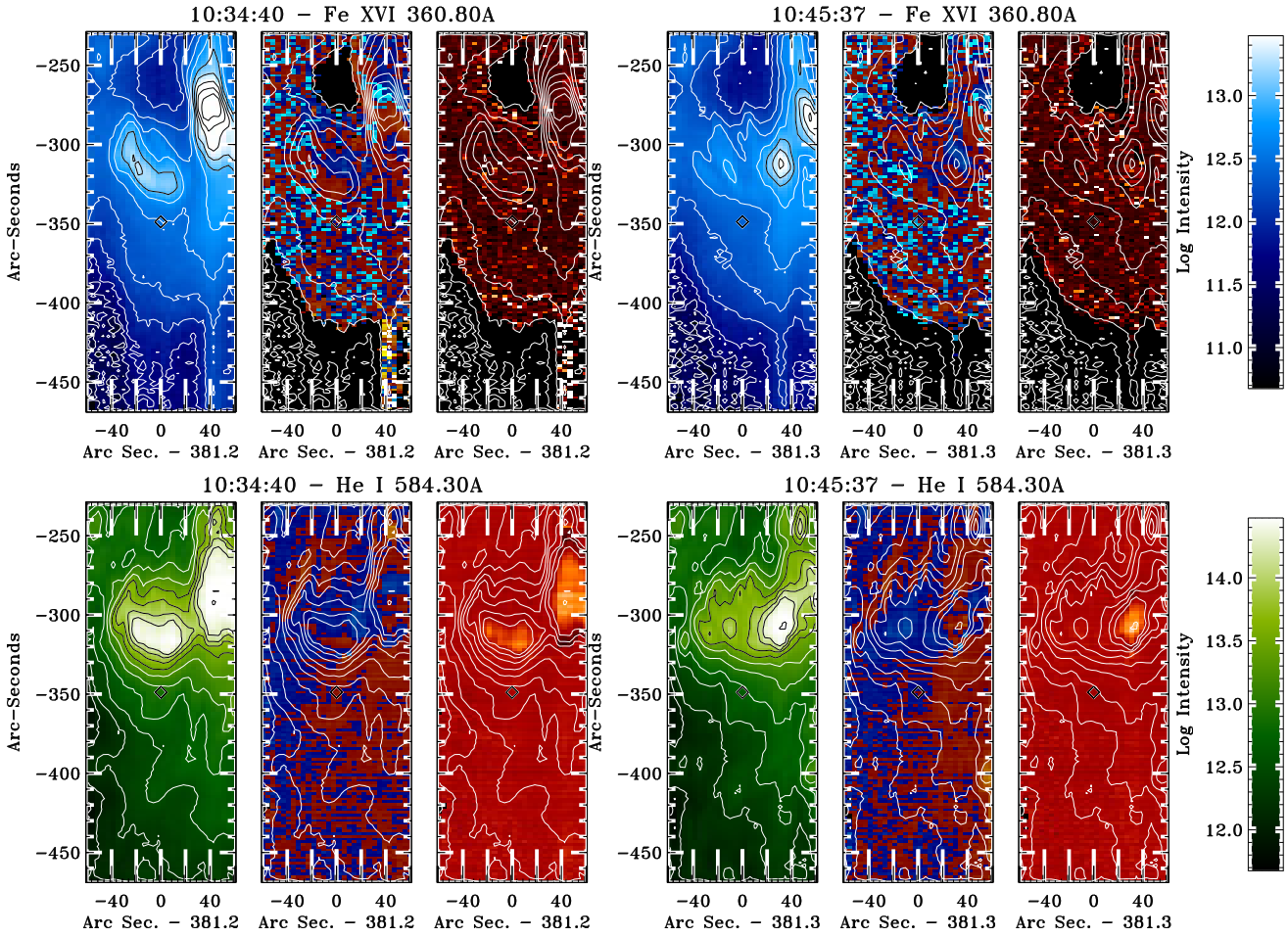

Fig. 5. Similar to Fig. 3, but the CDS rasters depict the Fe XVI 360.80 Å (*top row*) and He I 584.30 Å (*bottom row*) lines at 10:34:40 UT and 10:45:37 UT on 2002 August 19. Places in the Fe XVI image that were below a certain intensity threshold have not been fit. The velocity and FWHM panels use the same color tables as Fig. 3.

the mechanism of ion acceleration in reconnection exhausts (Drake et al. 2009) or cyclotron resonance with Alfvén waves (Kumar et al. 2017) that predict more efficient acceleration for ions with low Q/A. Note that O V and Fe XVI have almost identical Q/A and therefore should exhibit similar enhancement factor. However, no excess broadening was observed in the Fe XVI line in the examined event. Jeffrey et al. (2017) have found that broadened line profiles may arise from nonthermal Fe if ions are locally accelerated on timescales <0.1 s. Because of these stringent conditions, the authors suggest that more plausible explanation for the observed line profiles are non-Gaussian turbulent velocities, which was supported by the observations of low redshifts. Similarly, we observe a low redshift at sites with the excess line broadening that could drive the plasma turbulence that is responsible for the He I and O V line profiles.

Orrall & Zirker (1976) have shown that nonthermal neutral hydrogen H I may become excited and radiate Lyα. The authors pointed out that the effect can occur in the lines of other ions and atoms. Peter et al. (1990) have extended the calculations for a singly-ionized helium (He II). The authors give the charge-exchange cross sections for formations of He II from α-particle and of neutral He I from He II. The probability of the double charge-exchange process to form He I rapidly decreases with the energy increase in 50–400 keV nucleon^{-1}, implying that the effect would not be strong

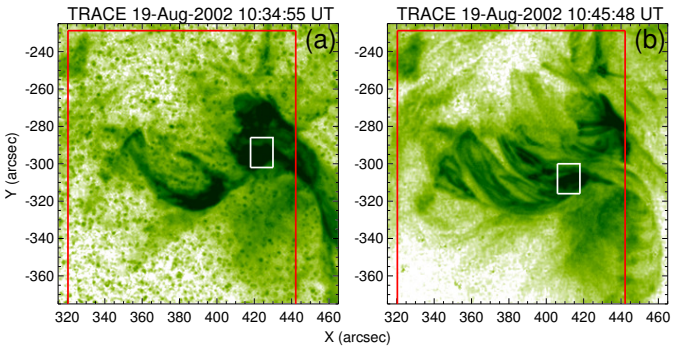

Fig. 6. TRACE 195 Å EUV direct images (in reverse color-scale, where dark corresponds to high intensities) of the source M2.1 flare in event 2 around the flare maximum (*panel a*) and ten minutes later (*panel b*). The red rectangles depict the CDS FOV. White rectangles mark pixels with enhanced line broadenings. *Panel a* shows the EIT flare in Fig. 1b at higher resolution. The noise spikes in the images are not filtered out.

in the He I line, but details on a formation of broadened line profiles from the energetic He I are unknown.

It has been thought that ions in ^{3}He-rich SEP events are accelerated in the impulsive phase of solar flares along with nonrelativistic electrons (Reames et al. 1985; Wang et al. 2012). Reames (1988) has suggested that ions are accelerated at the

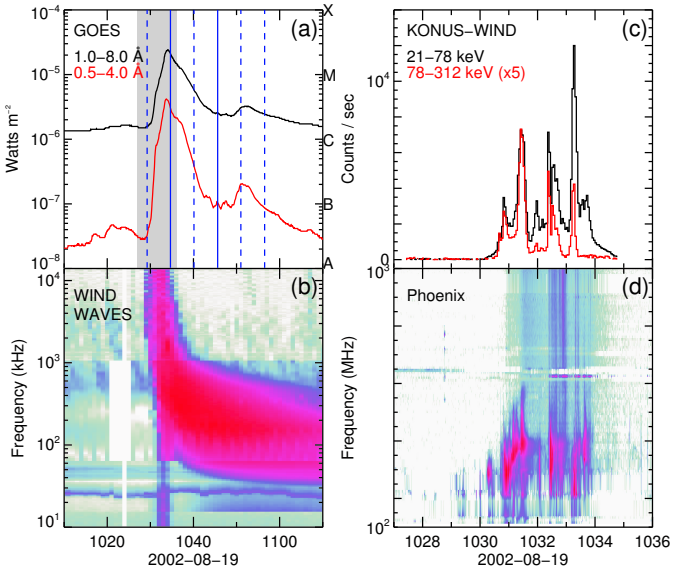

Fig. 7. *Panel a*: full-disk GOES-10 3 s X-ray fluxes. The labels A, B, C, M, and X on the right y-axis indicate flare classes in the 1–8 Å channel. The vertical lines mark the start times of six CDS rasters; two solid vertical lines indicate the starts of the rasters when the excess line broadening is observed. *Panel b*: Wind WAVES 1 min averaged radio spectra. *Panel c*: full-disk Wind KONUS 3 s averaged X-ray counts^{-1} in a 9-min period marked by the shaded bar in *panel a*. The 78–312 keV fluxes are multiplied by a factor of 5. *Panel d*: Phoenix 100 ms radio spectra.

time of HXR maximum. This might also be the case of event 2, where the ion and (the relativistic) electron injection times roughly coincide. In the examined event, the strongest line broadening was seen near the reconnection site of the jet, but at the time when the type III radio and HXR bursts terminated. This implies that the enhanced line broadening occurred at times when there was no energetic electron injection into interplanetary space or into the chromosphere. Unfortunately, this location was not scanned during the impulsive phase of the flare, although at the flare onset time, no line broadenings were seen. Nevertheless, the observed excess in the line broadening does not appear to be related to the wave turbulence that accelerated electrons (and presumably also the ions), otherwise energetic particle generation would continue.

Winglee (1989) has developed an acceleration mechanism related to the bulk flow evaporation, based on the ion-ion stream instability initiated by the precipitating energetic electrons. Although the observations in event 2 show a blueshift in the SEP source flare, the strongest blueshift was observed in the weaker follow-up recurrent X-ray flare (~15 min after the SEP event associated X-ray flare maximum) without a signature of particle acceleration. Reames et al. (1994) have doubted the mechanism as the events with chromospheric evaporation did not correlate with ^{3}He-rich flares. The question whether such mechanism could operate in ^{3}He-rich SEP flares remains still open, but it appears that the intensity of the blueshifted component alone may not be an appropriate indicator for the mechanism at work.

The diagnostic capabilities of EUV line spectroscopy for ion acceleration in solar flares need to be further explored, possibly with observations that have better temporal resolution. In the event examined here, the area around the jet locus was not scanned during the critical impulsive phase that lasted about 3–4 min. Thus, we do not know when the excess broadening started and how it evolved in time. For many flares, the excess broadening is observed to increase at the beginning of the impulsive phase (Fludra et al. 1989). Furthermore, near the flare onset, when the background from the flaring chromosphere is low and charge-exchange is more efficient as the medium is less ionized, the effect from the nonthermal ions may be better visible (Orrall & Zirker 1976; Peter et al. 1990). More recent spectroscopic observations are performed with the EIS and IRIS spectrometers. The EIS, in operation since November 2006, observes the solar corona at two wavelength bands, 170–210 Å and 250–290 Å with 0.06 Å spectral and 2″ spatial resolution over an FOV of up to 360″ × 512″ (Culhane et al. 2007). A preliminary check of the EIS flare catalog[4] indicates 10 out of 54 (January 2007–May 2014) already reported ^{3}He-rich SEP source flares (Nitta et al. 2015; Bučík et al. 2016) in the EIS FOV. The IRIS provides UV spectra and images around 1400 Å and 2800 Å that focus on the chromosphere with 0.03 Å spectral, 0.4″ spatial, and 2 s temporal resolution over an FOV of up to 175″ × 175″ (De Pontieu et al. 2014). So far, only 9 ^{3}He-rich flares in the Earth view have been reported (Nitta et al. 2015) that cover the observing period of IRIS (since July 2013), but none were found in the spectrograph FOV. An intentional pointing of the spectrometers to a candidate ^{3}He-rich SEPs source (such as an active region on a near-equatorial coronal hole boundary in the western hemisphere) might provide more events for a systematic investigation.

Acknowledgements. This work was supported by the Deutsche Forschungsgemeinschaft (DFG) under grant BU 3115/2–1 and the Max-Planck-Gesellschaft zur Förderung der Wissenschaften. ŠM acknowledges VEGA grant 2/0155/18.

References

Aptekar, R. L., Frederiks, D. D., Golenetskii, S. V., et al. 1995, Space Sci. Rev., 71, 265
Bougeret, J.-L., Kaiser, M. L., Kellogg, P. J., et al. 1995, Space Sci. Rev., 71, 231
Brosius, J. W. 2001, ApJ, 555, 435
Brosius, J. W., & Woodgate, B. E. 1999, ApJ, 514, 430
Bučík, R., Innes, D. E., Mall, U., et al. 2014, ApJ, 786, 71
Bučík, R., Innes, D. E., Mason, G. M., & Wiedenbeck, M. E. 2016, ApJ, 833, 63
Bučík, R., Innes, D. E., Mason, G. M., et al. 2018, ApJ, 852, 76
Cane, H. V., Richardson, I. G., & von Rosenvinge, T. T. 2010, J. Geophys. Res., 115, A08101
Canfield, R. C., & Chang, C.-R. 1985, ApJ, 295, 275
Chen, N.-H., Bučík, R., Innes, D. E., & Mason, G. M. 2015, A&A, 580, A16
Culhane, J. L., Harra, L. K., James, A. M., et al. 2007, Sol. Phys., 243, 19
Czaykowska, A., De Pontieu, B., Alexander, D., & Rank, G. 1999, ApJ, 521, L75
Delaboudinière, J. P., Artzner, G. E., Brunaud, J., et al. 1995, Sol. Phys., 162, 291
De Pontieu, B., Title, A. M., Lemen, J. R., et al. 2014, Sol. Phys., 289, 2733
Drake, J. F., Cassak, P. A., Shay, M. A., Swisdak, M., & Quataert, E. 2009, ApJ, 700, L16
Fleishman, G. D., & Toptygin, I. N. 2013, MNRAS, 429, 2515
Fludra, A. 2001, A&A, 368, 639
Fludra, A., Lemen, J. R., Jakimiec, J., Bentley, R. D., & Sylwester, J. 1989, ApJ, 344, 991
Fisk, L. A. 1978, ApJ, 224, 1048
Handy, B. N., Acton, L. W., Kankelborg, C. C., et al. 1999, Sol. Phys., 187, 229
Harrison, R. A., Sawyer, E. C., Carter, M. K., et al. 1995, Sol. Phys., 162, 233
Hudson, H. S., Fletcher, L., MacKinnon, A. L., & Woods, T. N. 2012, ApJ, 752, 84
Jeffrey, N. L. S., Fletcher L., & Labrosse, N. 2016, A&A, 590, A99
Jeffrey, N. L. S., Fletcher L., & Labrosse, N. 2017, ApJ, 836, 35
Kahler, S. W. 2007, Space Sci. Rev., 129, 359

[4] http://solarb.mssl.ucl.ac.uk/SolarB/eisflarecat.jsp

Kahler, S. W., Reames, D. V., & Sheeley Jr., N. R. 2001, ApJ, 562, 558
Kartavykh, Y. Y., Dröge, W., Klecker, B., et al. 2007, ApJ, 671, 947
Krucker, S., Larson, D. E., Lin, R. P., & Thompson, B. J. 1999, ApJ, 519, 864
Krucker, S., Kontar, E. P., Christe, S., Glesener, L., & Lin, R. P. 2011, ApJ, 742, 82
Kumar, R., Eichler, D., Gaspari, M., & Spitkovski, A. 2017, ApJ, 835, 295
Laming, J. M., Moses, J. D., Ko, Y.-K., et al. 2013, ApJ, 770, 73
Leske, R. A., Wiedenbeck, M. E., Cohen, C. M. S., et al. 2003, in Proc. 28th ICRC (Tsukuba), 6, 3253
Lin, R. P., Anderson, K. A., Ashford, S., et al. 1995, Space Sci. Rev., 71, 125
Liu, S., Petrosian, V., & Mason, G. M. 2006, ApJ, 636, 462
Mandzhavidze, N., Ramaty, R., & Kozlovsky, B. 1999, ApJ, 518, 918
Mason, G. M. 2007, Space Sci. Rev., 130, 231
Mason, G. M., Wiedenbeck, M. E., Miller, J. A., et al. 2002, ApJ, 574, 1039
Mason, G. M., Mazur, J. E., Dwyer, J. R., et al. 2004, ApJ, 606, 555
McComas, D. J., Bame, S. J., Barker, P., et al. 1998, Space Sci. Rev., 86, 563
Messmer, P., Benz, A. O., & Monstein, C. 1999, Sol. Phys., 187, 335
Miller, J. A. 1998, Space Sci. Rev., 86, 79
Milligan, R. O. 2011, ApJ, 740, 70
Milligan, R. O., Gallagher, P. T., Mathioudakis, M., & Keenan, F. P. 2006a, ApJ, 642, L169
Milligan, R. O., Gallagher, P. T., Mathioudakis, M., et al. 2006b, ApJ, 638, L117
Moortel, I. De., & Nakariakov, V. M. 2012, RSPTA, 370, 3193
Müller-Mellin, R., Kunow, H., Fleissner, V., et al. 1995, Sol. Phys., 162, 483
Murphy, R. J., Ramaty, R., Kozlovsky, B., & Reames, D. V. 1991, ApJ, 371, 793
Nitta, N. V., Reames, D. V., DeRosa M. L., et al. 2006, ApJ, 650, 438
Nitta, N. V., Mason, G. M., Wang, L., Cohen, C. M. S., & Wiedenbeck, M. E. 2015, ApJ, 806, 235
Orrall, F. Q., & Zirker, J. B. 1976, ApJ, 208, 618
Peter, Th., Ragozin, E. N., Urnov, A. M., Uskov, D. B., & Rust, D. M. 1990, ApJ, 351, 317
Reames, D. V. 1988, ApJ, 325, L53
Reames, D. V., & Ng, C. K. 2004, ApJ, 610, 510
Reames, D. V., & Stone, R. G. 1986, ApJ, 308, 902
Reames, D. V., von Rosenvinge, T. T., & Lin, R. P. 1985, ApJ, 292, 716
Reames, D. V., Dennis, B. R., Stone, R. G., & Lin, R. P. 1988, ApJ, 327, 998
Reames, D. V., Meyer, J. P., & von Rosenvinge, T. T. 1994, ApJS, 90, 649
Reames, D. V., Cliver, E. W., & Kahler, S. W. 2014, Sol. Phys., 289, 3817
Scherrer, P. H., Bogart, R. S., Bush, R. I., et al. 1995, Sol. Phys., 162, 129
Shibata, K., Ishido, Y., Acton, L. W., et al. 1992, PASJ, 44, L173
Smith, C. W., L'Heureux, J., Ness, N. F., et al. 1998, Space Sci. Rev., 86, 613
Tan, C., & Yan, Y. 2008, Adv. Space Res., 41, 992
Temerin, M., & Roth, I. 1992, ApJ, 391, L105
Teriaca, L., Falchi, A., Falciani, R., Cauzzi, G., & Maltagliati, L. 2006, A&A, 455, 1123
Van Hollebeke, M. A. I., McDonald, F. B., & Meyer, J. P. 1990, ApJS, 73, 285
Vilmer, N., MacKinnon, A. L., & Hurford, G. J. 2011, Space Sci. Rev., 159, 167
Wang, Y.-M., Pick, M., & Mason, G. M. 2006, ApJ, 639, 495
Wang, L., Lin, R. P., Krucker, S., & Mason, G. M. 2012, ApJ, 759, 69
Wiedenbeck, M. E., Cohen, C. M. S., Leske, R. A., et al. 2010, ApJ, 719, 1212
Winglee, R. M. 1989, ApJ, 343, 511
Woodgate, B. E., Robinson, R. D., Carpenter, K. G., Maran, S. P., & Shore, S. N. 1992, ApJ, 397, L95
Zhang, T. X. 2004, ApJ, 617, L77